Device Simulation of Negative-Capacitance Field-Effect Transistors With a Ferroelectric Gate Insulator

Junichi Hattori, Tsutomu Ikegami, Koichi Fukuda, Hiroyuki Ota, Shinji Migita, and Hidehiro Asai
National Institute of Advanced Industrial Science and Technology (AIST), Tsukuba, Ibaraki 305-8568, Japan
E-mail: j.hattori@aist.go.jp

***Abstract*—We consider the method to simulate negative-capacitance field-effect transistors having a ferroelectric film as a gate insulator in the framework applicable to technology computer-aided design device simulators and propose a method with complete applicability. In the method, the behavior of the polarization in ferroelectrics is described by the Landau–Khalatnikov equation and it is solved simultaneously with the Poisson equation to obtain the distribution of the polarization and electrostatic potential. Also, the proposed method enables the device simulators to take into account a factor related to forming domain structures of the polarization.**

***Index Terms*—TCAD, device simulation, negative capacitance, ferroelectrics**

I. Introduction

Integrated circuits have been strongly required to reduce their power consumption for portable, wearable, implantable, and wireless sensor network applications. An effective way is to lower the operating voltage. To this purpose, constituent transistors should be switched on and off within a narrow input voltage range. Negative-capacitance (NC) field-effect transistors (FETs) exploiting the NC state of ferroelectric materials have been proposed as such steep switching transistors [1]. The ferroelectric film inserted in the gate stack as a gate insulator reduces the voltage applied to the underlying structure at a low gate voltage V_{G}, while enhances it at a high V_{G}. Owing to this V_{G} modulation, the structure beneath the ferroelectric film experiences a larger variation in the applied voltage than a given variation in V_{G} and consequently the drain current steeply increases or decreases. NC FETs have recently been studied intensively and their steep witching has already been reported by a number of research groups [2]–[4]. To support and promote such studies, the establishment of simulation method for NC FETs is urgently needed.

In the previous representative method [5]–[9], which implicitly targets NC FETs having a metal film beneath a ferroelectric film, the behavior of the ferroelectric capacitor sandwiched between the internal metal film and gate electrode and that of the remaining transistor structure are simulated separately and then the results obtained for the transistor are corrected by the voltage across the capacitor. Although this method uses the assumption that the polarization is uniform in ferroelectrics, several methods taking into account the distribution of the polarization have recently been proposed [10], [11]. Device simulator in technology computer-aided design (TCAD) system is a de facto standard for the simulation of electronic devices' behavior. Although in the former method the simulator is usually used for the simulation of the transistor part [5]–[8], to fully incorporate the method into the simulator seems to be difficult due to the differences in the simulation framework and algorithm, which applies to the latter method.

We have developed our own device simulator, Impulse TCAD [12], and realized the simulation of NC FETs, thereby revealing their interesting features such as reverse drain-induced barrier lowering, negative drain conductance, and fringing field effect [13]–[15]. In this work, we consider the way for TCAD device simulators to properly simulate NC FETs' behavior. In the simulation of NC FETs, the polarization field of ferroelectrics is described by the Poisson and Landau–Khalatnikov equations. We discuss the discretization methods of these equations and propose a method completely applicable to the device simulators. The method also has high extensibility, which allows us to easily introduce ferroelectrics' feature of polarization vectors to align with each other into the simulation.

II. Theory

A. Device Simulation

In a typical device simulation, the electrostatic potential distribution $\psi(\boldsymbol{r})$ in a target device is described by the following Poisson equation,

$$\nabla \cdot [\varepsilon(\boldsymbol{r})\boldsymbol{E}(\boldsymbol{r})] - \rho(\boldsymbol{r}) = 0, \tag{1}$$

where $\varepsilon(\boldsymbol{r})$ and $\rho(\boldsymbol{r})$ are the permittivity and charge density at the position $\boldsymbol{r}$, respectively, and $\boldsymbol{E}(\boldsymbol{r})$ is the electric field and is given by $\boldsymbol{E}(\boldsymbol{r}) = -\nabla\psi(\boldsymbol{r})$. Also, the concentration distributions of electrons and holes are governed by the continuity equations of their currents. As the first step to solve these three equations, a device simulator discretizes them using a finite volume scheme. In the scheme, the target device is divided into finite volumes referred to as control volumes and associated with each of the nodes of a computational mesh. In this study, the control volume of a node is assumed to be bounded by planes, each of which is perpendicular to the edge between the node and an adjacent node and is passing through the midpoint of the edge, as shown in Fig. 1. Representing the values of parameters and variables in a control volume by those at its owner node and integrating an equation over

978-1-5386-6790-3/18/$31.00 ©2018 IEEE

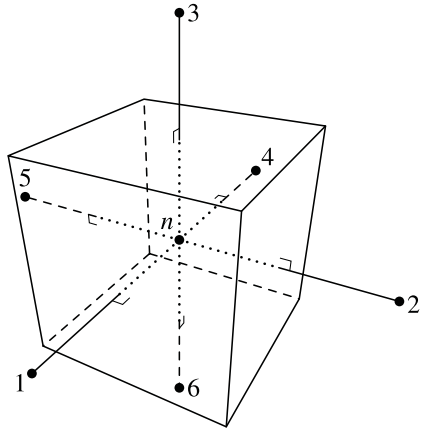

Fig. 1. Schematic view of the control volume of a node n, each of whose faces is perpendicular to the edge between the node and an adjacent node and is passing through the midpoint of the edge.

the control volume, we can derive the discretized form of the equation. For example, the discretized Poisson equation (1) for the nth node can be written as

$$\sum_m \varepsilon_n E_{nm} S_{nm} - \rho_n V_n = 0, \tag{2}$$

where the summation over m is taken for all adjacent nodes, V_n is the volume of the nth node's control volume, and S_{nm} is the area of the face of V_n intersecting with the edge from the nth to the mth node $\boldsymbol{r}_{nm}$. Also, E_{nm} denotes the component of the electric field on S_{nm} along $\boldsymbol{r}_{nm}$ and can be approximated as $E_{nm} = -(\psi_m - \psi_n)/\ell_{nm}$ with ℓ_{nm} being the length of $\boldsymbol{r}_{nm}$. In this way, the Poisson and two current continuity equations are rewritten as a lot of equations having the electrostatic potential and electron and hole concentrations at each nodes as variables, and then the device simulator solves them to determine the variables' values using the Newton–Raphson method. Concretely, when the equations are written together as $f(\boldsymbol{v}) = \boldsymbol{0}$, the difference between the very solution $\boldsymbol{v}_\infty$ and its guess value $\boldsymbol{v}_0$ can be estimated from the following equation,

$$\frac{\partial f(\boldsymbol{v}_0)}{\partial \boldsymbol{v}} \Delta \boldsymbol{v} = -f(\boldsymbol{v}_0). \tag{3}$$

The sum of $\boldsymbol{v}_0$ and the estimated difference value $\Delta \boldsymbol{v}$ is expected to approach $\boldsymbol{v}_\infty$ compared to $\boldsymbol{v}_0$. Thus, repeatedly solving this equation while updating $\boldsymbol{v}_0$, we can obtain a $\boldsymbol{v}$'s value sufficiently close to $\boldsymbol{v}_\infty$.

B. Ferroelectrics

We described the behavior of the polarization $\boldsymbol{P} = (P_x, P_y, P_z)$ in a ferroelectric material using the Landau–Khalatnikov model [16],

$$\lambda \frac{\partial P_i}{\partial t} = -\frac{\partial G}{\partial P_i} \quad (i = x, y, z), \tag{4}$$

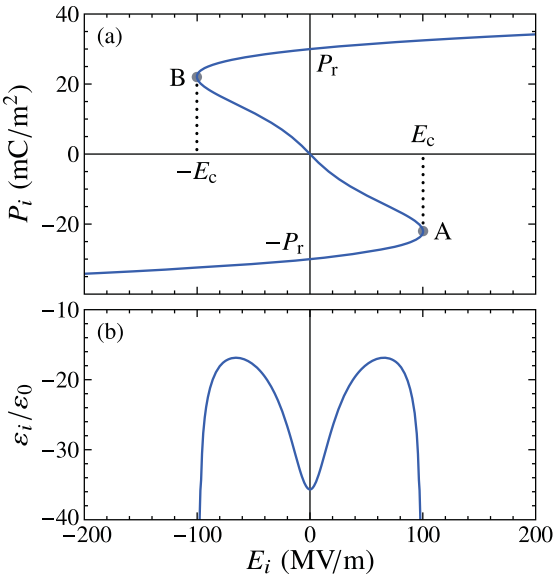

Fig. 2. (a) Polarization along each axis in the considered ferroelectric material plotted as a function of the electric field. NC states lie on the A–B line. (b) Permittivity normalized by that of vacuum and calculated for the NC states.

where λ is the material parameter related to the mobility of domain walls and G is the Gibbs free energy. In the Landau–Devonshire model [17], its density can be written as

$$\begin{aligned} g(\boldsymbol{r}) = {} & \alpha(P_x^2 + P_y^2 + P_z^2) + \beta(P_x^4 + P_y^4 + P_z^4) \\ & + \gamma(P_x^6 + P_y^6 + P_z^6) - \boldsymbol{E} \cdot \boldsymbol{P}, \end{aligned} \tag{5}$$

where α, β, and γ are the material parameters. In a steady state, (4) is rewritten as

$$2\alpha P_i + 4\beta P_i^3 + 6\gamma P_i^5 - E_i = 0 \quad (i = x, y, z). \tag{6}$$

Fig. 2(a) shows this relationship between $\boldsymbol{P}$ and $\boldsymbol{E}$ in the considered ferroelectric material, whose α, β, and γ were respectively set to $-1.54 \times 10^9\,\mathrm{m/F}$, $-2.65 \times 10^{12}\,\mathrm{m^5/FC^2}$, and $2.60 \times 10^{15}\,\mathrm{m^9/FC^4}$ so that the remanent polarization P_r and coercive electric field E_c are about $3 \times 10^{-3}\,\mathrm{C/m^2}$ and $100 \times 10^6\,\mathrm{V/m}$. In the figure, the ferroelectric material is in an NC state on the A–B line and its permittivity has a negative value, as shown in Fig. 2(b).

Solving (6) together with the Poisson equation (1), we can obtain $\psi(\boldsymbol{r})$ in the ferroelectric material. In doing so, to handle $\boldsymbol{P}$ independently of $\boldsymbol{E}$, (1) was modified as follows:

$$\nabla \cdot [\varepsilon_0 \boldsymbol{E}(\boldsymbol{r}) + \boldsymbol{P}(\boldsymbol{r})] - \rho(\boldsymbol{r}) = 0, \tag{7}$$

where ε_0 is the permittivity of vacuum. In addition, the charge density $\rho(\boldsymbol{r})$ was set to 0.

III. Results and Discussion

A. Decoupled Solution

The discretized form of (7) can be written as

$$\sum_m (\varepsilon_0 E_{nm} + P_{nm}) S_{nm} - \rho_n V_n = 0, \tag{8}$$

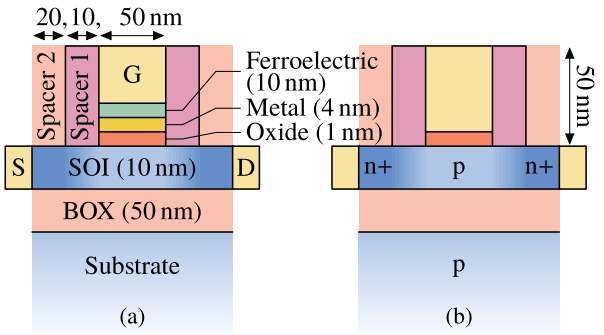

Fig. 3. (a) Schematic view of an NC FET. The regions labeled "G", "S", and "D" represent the gate, source, and drain electrodes, respectively. The thicknesses of the film components are shown in parentheses in their labels. (b) Schematic view of the corresponding MOS FET, which is obtained from the NC FET by replacing the ferroelectric and internal metal films with the gate electrode.

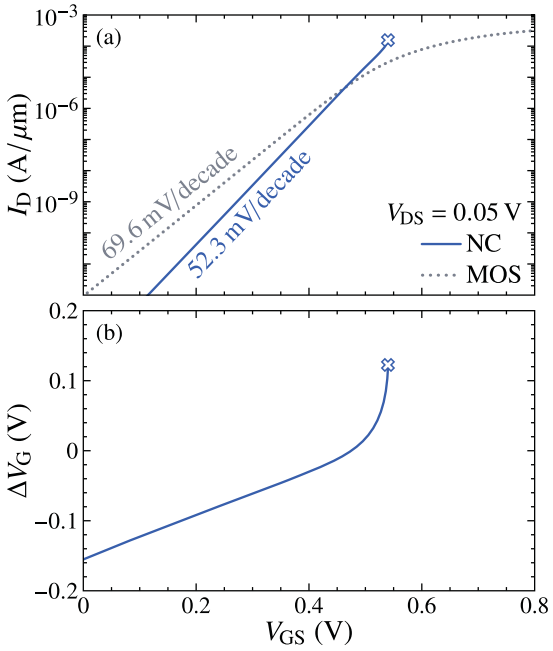

Fig. 4. (a) I_D–V_{GS} characteristics of (solid line) the NC and (dotted line) MOS FETs shown in Figs. 3(a) and 3(b). The simulation was conducted for a drain-to-source voltage V_{DS} of 0.05 V. (b) Voltage across the ferroelectric film or gate voltage modulation ΔV_G of the NC FET plotted as a function of V_{GS}.

where P_{nm} is the component of the polarization on the control volume's face S_{nm}, $\boldsymbol{P}_{nm}$, along the edge $\boldsymbol{r}_{nm}$ and is given by $P_{nm} = \boldsymbol{P}_{nm} \cdot \boldsymbol{u}_{nm}$ with $\boldsymbol{u}_{nm}$ being the unit vector of $\boldsymbol{r}_{nm}$. The determination of $\boldsymbol{P}_{nm}$ is the key issue in the simulation of NC FETs. A straightforward way is to approximate the electric field on S_{nm}, $\boldsymbol{E}_{nm}$, as $\boldsymbol{E}_{nm} = E_{nm}\boldsymbol{u}_{nm}$ and then solve (6) for each component of $\boldsymbol{P}_{nm}$ with the corresponding component of $\boldsymbol{E}_{nm}$.

We at first adopt this approach and simulated the NC FET having an internal metal film depicted in Fig. 3(a). The resulting drain current I_D vs gate-to-source voltage V_{GS} characteristic is shown in Fig. 4(a). The figure also shows the I_D–V_{GS} characteristic of the corresponding metal–oxide–semiconductor (MOS) FET depicted in Fig. 3(b). Comparing the two I_D–V_{GS} characteristics, we can see that the I_D of the NC FET increases more steeply. This is due to the gate voltage modulation by the NC of the ferroelectric film, which is shown in Fig. 4(b). The figure shows the difference between the electrostatic potentials at the lower and upper interfaces of the ferroelectric film, ΔV_G, plotted as a function of V_{GS} and indicates that the NC works as expected. In other words, it reduces the voltage applied to the MOS structure underlying the ferroelectric film at a low V_{GS}, while at a high V_{GS} it enhances the voltage. It is note that the cross marks in Fig. 4 show the device state just before the gate capacitance becomes negative and consequently the simulation is terminated.

B. Coupled Solution

In the approach described in the previous subsection, (6) is solved separately from the Poisson and current continuity equations, that is, it is not included in the equation $f(\boldsymbol{v}) = \boldsymbol{0}$ mentioned in Section II-A and is solved when the vector $f(\boldsymbol{v})$ and the Jacobian $\partial f(\boldsymbol{v}_0)/\partial \boldsymbol{v}$ are being constructed to solve (3). Fortunately, as long as the electric field is smaller than E_c in the ferroelectric film, (6) can be easily solved by using the Newton method and the assumption that the film is in an NC state. However, a device simulator should have an error handler for the failure of solving (6). Such special treatments of (6) would be a burden to the device simulator in terms of the maintainability and extensibility. For example, when cross terms of the polarization components such as $P_x^2 P_y^2$ are added to the Gibbs free energy density, the three equations of (4) should be solved simultaneously to determine the three components. Also, in a transient simulation, the device simulator should store the polarization distributions in previous time points, although a polarization vector is associated with not a node but an edge and the data structure of its distribution is more complicated than that of the distribution of the electrostatic potential or carrier concentration.

To avoid these issues, there is no alternative but to include (6) in $f(\boldsymbol{v}) = \boldsymbol{0}$, which become possible by treating a polarization vector as a property of each nodes similarly to the electrostatic potential and carrier concentration and representing the polarization vector in a control volume by that at its owner node $\boldsymbol{P}_n = (P_{x,n}, P_{y,n}, P_{z,n})$. Then, P_{nm} in (8) is given by $P_{nm} = P_n \cdot \boldsymbol{u}_{nm}$ and (6) can be discretized for the nth node as follows:

$$(2\alpha P_{i,n} + 4\beta P_{i,n}^3 + 6\gamma P_{i,n}^5 - E_{i,n})V_n = 0 \quad (i = x, y, z). \quad (9)$$

Here, $E_{i,n}$ is the electric field component along the i-axis at the nth node and is approximated as

$$E_{i,n} = \frac{\sum_m E_{nm} u_{i,nm} S_{nm} |u_{i,nm}|}{\sum_m S_{nm} |u_{i,nm}|} \quad (i = x, y, z) \qquad (10)$$

with $u_{i,nm}$ begin the component of $\boldsymbol{u}_{nm}$ along the i-axis. Equation (9) and $\boldsymbol{P}_n$ can be included in $f(\boldsymbol{v}) = \boldsymbol{0}$ and $\boldsymbol{v}$,

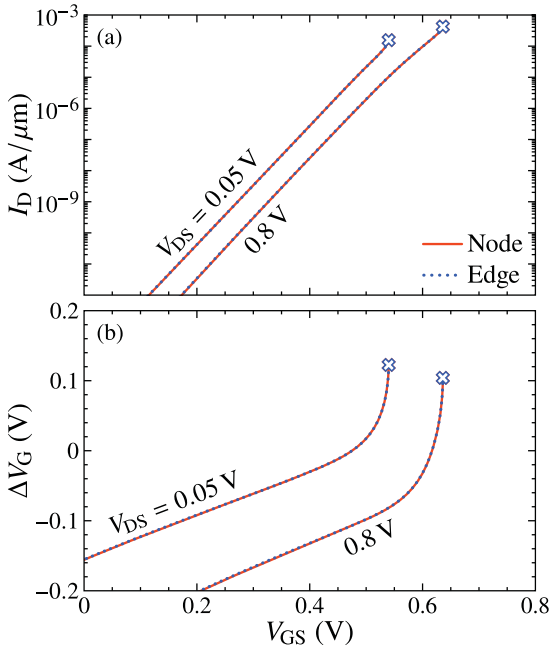

Fig. 5. (a) I_D and (b) ΔV_G in NC FETs calculated as a function of V_{GS} using the methods described in (solid line) Sections III-B and (dotted line) III-A.

respectively, and a device simulator can solve (6) together with the Poisson and current continuity equations. The device simulator is flexible to some extent about this kind of function enhancement because in some cases it is required to simulate the lattice and carrier temperatures in addition to the electrostatic potential and carrier concentration at each node and it may be designed with this requirement in mind.

Fig. 5(a) shows the I_D–V_{GS} characteristics of NC FETs calculated using the approaches mentioned above and in the previous subsection and indicates that the two approaches have a comparable accuracy. This is also confirmed in ΔV_G shown in Fig. 5(b) and the polarization field shown in Figs. 6(a) and 6(b).

C. Domain Structures

The polarization fields in the ferroelectric film shown in Figs. 6(a) and 6(b) vary considerably in the thickness direction near both gate edges and do not look like ferroelectrics because the well-known tendency of polarization vectors to align with each other is not observed. Such tendency can be realized by introducing the penalty for the spatial variation in the polarization into the Gibbs free energy density (5), which for cubic materials is written as [18], [19],

$$\begin{aligned} g_{\rm dw}(\boldsymbol{r}) = {} & \frac{\delta_{11}}{2}({P'_{x,x}}^2 + {P'_{y,y}}^2 + {P'_{z,z}}^2) \\ & + \delta_{12}(P'_{x,x}P'_{y,y} + P'_{y,y}P'_{z,z} + P'_{z,z}P'_{x,x}) \\ & + \frac{\delta_{44}}{2}\left[(P'_{x,y} + P'_{y,x})^2 + (P'_{y,z} + P'_{z,y})^2 \right. \\ & \left. + (P'_{z,x} + P'_{x,z})^2\right]. \end{aligned} \tag{11}$$

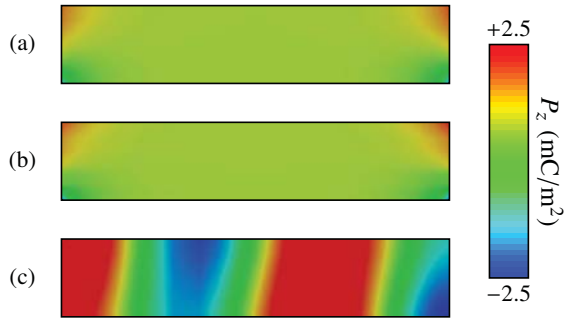

Fig. 6. Distribution of the z-component of the polarization in the ferroelectric film of NC FETs calculated using the methods described in (a) Sections III-A, (b) III-B, and (c) III-C at V_{GS} of 0.4 V and V_{DS} of 0.05 V. In (c), δ was set so that the domain wall thickness T_{dw} is 10 nm.

Here, $P'_{i,j}$ represent $\partial P_i/\partial x_j$ ($x_1 = x$, $x_2 = y$, and $x_3 = z$) and δ_{11}, δ_{12}, and δ_{44} are the material parameters related to the thickness of domain walls. Taking this term into account and assuming that $\delta_{11} = -\delta_{12} = \delta_{44} = \delta$, we can rewrite (6) as

$$\begin{aligned} & 2\alpha P_i + 4\beta P_i^3 + 6\gamma P_i^5 - E_i \\ & \qquad - \delta\nabla\cdot(\nabla P_i) = 0 \end{aligned} \quad (i = x, y, z). \tag{12}$$

Fortunately, since this equation has the same form as the Poisson and current continuity equations, its discretized form would be derived without difficulty and we adopted the following form,

$$\begin{aligned} & \sum_m \delta\frac{P_{i,n} - P_{i,m}}{\ell_{nm}}S_{nm} + (2\alpha P_{i,n} \\ & \quad + 4\beta P_{i,n}^3 + 6\gamma P_{i,n}^5 - E_{i,n})V_n = 0 \end{aligned} \quad (i = x, y, z). \tag{13}$$

The I_D and ΔV_G in NC FETs having a ferroelectric film with non-zero or zero δ are shown in Figs. 7(a) and 7(b), respectively. In the simulation, the non-zero δ value was chosen so that the domain wall thickness T_{dw} is 10 nm, which is given by [19]

$$T_{\rm dw} = P_{\rm r}\sqrt{\frac{2\delta}{\beta P_{\rm r}^4 + 2\gamma P_{\rm r}^6}}. \tag{14}$$

Here, the remanent polarization P_r satisfies

$$P_{\rm r}^2 = \frac{-\beta + \sqrt{\beta^2 - 3\alpha\gamma}}{3\gamma}. \tag{15}$$

Figs. 6(c) and 6(b) show the polarization fields in the ferroelectric films with non-zero and zero δ's, respectively. In the case of zero δ, a variation in the polarization is concentrated at the film edges. On the other hand, in the case of non-zero δ, such a variation spreads throughout the film due to $g_{\rm dw}(\boldsymbol{r})$ and a domain structure appears. We have confirmed that the domain size increases with increasing δ. Although the introduction of $g_{\rm dw}(\boldsymbol{r})$ drastically changes the polarization field, such a noticeable change is not observed in the behaviors of NC FETs and ferroelectric films, as shown in Fig. 7. Even when a domain structure appears, upward and downward polarizations do not completely cancel each other out because

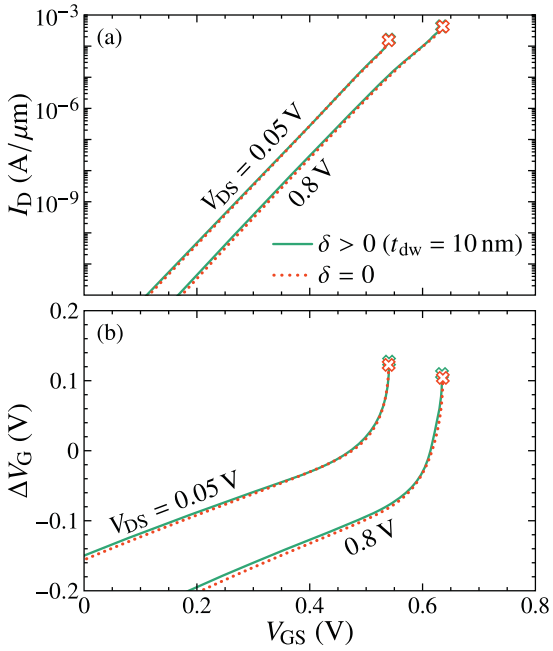

Fig. 7. (a) I_D and (b) ΔV_G in NC FETs having ferroelectric films with (solid line) non-zero and zero δ's. The non-zero δ was set so that $T_{dw} = 10$ nm.

of the differences in the magnitude and domain size, which reproduce the function of NC.

Since NC states are likely to stably appear in single domain structures [20], the internal metal film is expected to uniformly apply an electric field to the ferroelectric film, thereby aligning the directions of the polarization and facilitating the appearance of the NC states. However, the appearance of the multi domain structure shown in Fig. 6(c) implies that the internal metal film may not play the expected role in NC FETs. We have confirmed that the behavior of NC FETs without the internal metal film can be simulated relatively stably if $\delta$is large to some extent. Fig. 8 shows the I_D–V_{GS} characteristics of NC FETs without and with the internal metal films and indicates that the NC FETs lost the steep switching feature together with the film. We will discuss this interesting result elsewhere.

IV. Conclusions

In this work, we have studied the method to simulate NC FETs having a gate insulator film made of a ferroelectric material in the framework of TCAD device simulation. We adopt the Landau–Khalatnikov equation to describe the behavior of the polarization in ferroelectrics and proposed a method to solve this equation simultaneously with standard equations describing electronic devices' behavior. The method has been incorporated into our own device simulator and it has been confirmed by the simulator that the method can simulate NC FETs with an accuracy comparable to another method which solves the Landau–Khalatnikov equation separately from the other equations. Owing to its applicability to various

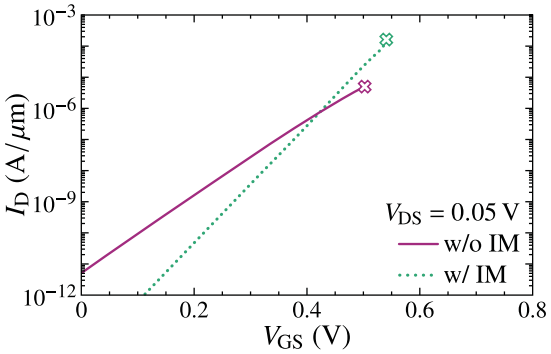

Fig. 8. I_D–V_{GS} characteristics of NC FETs without the internal metal film, which is merged into the gate oxide film while maintaining its capacitance. The results obtained for NC FETs with the internal metal film are also shown by the dotted line. The simulation was carried out for T_{dw} of 10 nm.

ferroelectric models, we successfully introduced a factor describing the tendency of polarization vectors to align with each other in ferroelectrics into the simulation and consequently observed that domain structures of the polarization appear in the ferroelectric film of NC FETs even when the film is sandwiched between the internal metal film and gate electrode. The proposed method will be helpful to improve the device simulation and then promote the research and development of NC FETs.

References

[1] S. Salahuddin and S. Datta, "Use of negative capacitance to provide voltage amplification for low power nanoscale devices," Nano Lett., vol. 8, no. 2, pp. 405–410, Dec. 2008.

[2] Z. Krivokapic, U. Rana, R. Galatage, A. Razavieh, A. Aziz, J. Liu, J. Shi, H. J. Kim, R. Sporer, C. Serrao, A. Busquet, P. Polakowski, J. Müller, W. Kleemeier, A. Jacob, D. Brown, A. Knorr, R. Carter, and S. Banna, "14nm ferroelectric FinFET technology with steep subthreshold slope for ultra low power applications," in Proc. IEEE Int. Electron Device Meeting (IEDM), Dec. 2017, pp. 357–360.

[3] J. Li, J. Zhou, G. Han, Y. Liu, Y. Peng, J. Zhang, Q.-Q. Sun, D. W. Zhang, and Y. Hao, "Negative capacitance Ge PFETs for performance improvement: impact of thickness of $HfZrO_x$," IEEE Trans. Electron Devices, vol. 65, no. 3, pp. 1217–1222, Mar. 2018.

[4] T. Srimani, G. Hills, M. D. Bishop, U. Radhakrishna, A. Zubair, R. S. Park, Y. Stein, T. Palacios, D. Antoniadis, and M. M. Shulaker, "Negative capacitance carbon nanotube FETs," IEEE Electron Device Lett., vol. 39, no. 2, pp.304–307, Feb. 2018.

[5] A. I. Khan, C. W. Yeung, C. Hu, and S. Salahuddin, "Ferroelectric negative capacitance MOSFET: capacitance tuning & antiferroelectric operation," in Proc. IEEE Int. Electron Device Meeting (IEDM), Dec. 2011, pp. 255–258.

[6] H. Ota, S. Migita, J. Hattori, K. Fukuda, and A. Toriumi, "Material and device engineering in fully depleted silicon-on-insulator transistors to realize a steep subthreshold swing using negative capacitance," Jpn. J. Appl. Phys., vol. 55, no. 4S, pp. 08PD01(1–5), Apr. 2016.

[7] A. Saeidi, F. Jazaeri, I. Stolichnov, and A. M. Ionescu, "Double-gate negative-capacitance MOSFET with PZT gate-stack on ultra thin body SOI: an experimentally calibrated simulation study of device performance," IEEE Trans. Electron Devices, vol. 63, no. 12, pp. 4678–4684 Dec. 2016.

[8] H. Ota, S. Migita, J. Hattori, K. Fukuda, and A. Toriumi, "Structural advantages of silicon-on-insulator FETs over FinFETs in steep subthreshold-swing operation in ferroelectric-gate FETs," Jpn. J. Appl. Phys., vol. 56, no. 4S, pp. 04CD10(1–4), Mar. 2017.

[9] J. Seo, J. Lee, and M. Shin, "Analysis of drain-induced barrier rising in short-channel negative-capacitance FETs and its applications," IEEE Trans. Electron Devices, vol. 64, no. 4, pp. 1793–1798, Apr. 2017.

[10] P. Lenarczyk and M. Luisier, "Physical modeling of ferroelectric field-effect transistors in the negative capacitance regime," in Proc. Int. Conf. Simulation of Semiconductor Processes and Devices (SISPAD), Sept. 2016, pp. 311–314
[11] A. K. Saha, P. Sharma, I. Dabo, S. Datta, and S. K. Gupta, "Ferroelectric transistor model based on self-consistent solution of 2D Poisson's, non-equilibrium Green's function and multi-domain Landau Khalatnikov equations," in Proc. IEEE Int. Electron Device Meeting (IEDM), Dec. 2017, pp. 326–329.
[12] ImpulseTCAD, National Institute of Advanced Industrial Science and Technology (AIST); https://unit.aist.go.jp/neri/intra/en/ImpulseTCAD/
[13] H. Ota, T. Ikegami, J. Hattori, K. Fukuda, S. Migita, and A. Toriumi, "Fully coupled 3-D device simulation of negative capacitance FinFETs for Sub 10 nm Integration," in Proc. IEEE Int. Electron Device Meeting (IEDM), Dec. 2016, pp. 318–321.
[14] H. Ota, K. Fukuda, T. Ikegami, J. Hattori, H. Asai, S. Migita, and A. Toriumi, "Perspective of negative capacitance FinFETs investigated by transient TCAD simulation," in Proc. IEEE Int. Electron Device Meeting (IEDM), Dec. 2017, pp. 361–364.
[15] J. Hattori, K. Fukuda, T. Ikegami, H. Ota, S. Migita, H. Asai, and A. Toriumi, "Fringing field effects in negative capacitance field-effect transistors with a ferroelectric gate insulator," Jpn. J. Appl. Phys., vol. 57, no. 4S, pp. 04FD07(1–7), Mar. 2018.
[16] L. D. Landau and I. M. Khalatnikov, "On the anomalous absorption of sound near a second order phase transition point," Dokl. Akad. Nauk SSSR, vol. 96, pp. 469–472, 1954.
[17] A. F. Devonshire, "XCVI. theory of barium titanate," Philos. Mag., vol. 40, pp. 1040–1063, 1949.
[18] V. L. Ginzburg and L. D. Landau, "On the Theory of superconductivity," Zh. Exp. Theor. Fiz., vol. 20, pp. 1064–1082, 1950.
[19] P. Marton, I. Rychetsky, and J. Hlinka, "Domain walls of ferroelectric $BaTiO_3$ within the Ginzburg-Landau-Devonshire phenomenological model," Phys. Rev. B, vol. 81, no. 14, pp. 144125(1–11), Apr. 2010.
[20] S. Kasamatsu, S. Watanabe, C. S. Hwang, and S. Han, "Emergence of negative capacitance in multidomain ferroelectric–paraelectric nanocapacitors at finite bias," Adv. Mater., vol. 28, nom 2, pp. 335–340, Jan. 2016.